Electronic Supplementary Material (ESI) for Soft Matter

Supporting Material (ESI)

Strain propagation in artificial extracellular matrix proteins can accelerate cell spreading and polarization

Shelly Tzlil[a] and David A. Tirrell[a,b]

[a]Division of Chemistry and Chemical Engineering, [b]Joseph J. Jacobs Institute for Molecular Engineering for Medicine, California Institute of Technology, Pasadena, CA 91125 (USA)

SI Text

Materials and Methods:

Microrheology.

Sample preparation: Samples for microrheology measurements were composed of three layers. The layers were spin-coated sequentially; samples were stored for 8 h at 4°C between coating steps. BS3-protein solutions (50 μL) were spin-coated as the bottom and top layers. BS3-protein solution (100 μL) mixed with 2×10^9 40-nm carboxylate-modified fluorescent beads (580/605 F8793, Invitrogen) was used for the central layer. All three layers had the same ratio of lysine residues to BS3 activated esters and all were spin-coated at 3000 RPM for 45 sec.

Microrheology measurement: Fluorescent beads were imaged over 1 min at an acquisition rate of 30 frames per second. Bead position was found by fitting a 2D Gaussian to the intensity image (1, 2). Bead displacement from time zero was averaged over all the beads in the same field of view (10-20 beads per field of view). The average displacement was fitted to a linear curve to extract the microscope drift. An alternative method that gave identical results is using image registration (enabling translation and rotation) to calculate the transformation between the first and last image in the time series and treat it as the drift. At least 10 fields of view were acquired per surface. Moduli were calculated from the average mean square displacement by using the approximate solution (3-5)

$$G'(\omega) = \left|G^*(\omega)\right| \cos\left(\frac{\pi\alpha(\omega)}{2}\right) \qquad [S1]$$

$$G''(\omega) = \left|G^*(\omega)\right| \sin\left(\frac{\pi\alpha(\omega)}{2}\right) \qquad [S2]$$

$$\left|G^*(\omega)\right| = \frac{2k_BT}{3\pi a\left\langle \Delta r^2\left(1/\omega\right)\right\rangle \Gamma\left(1+\alpha(\omega)\right)} \qquad [S3]$$

where Γ is the gamma function, $\omega = 1/t$ and $\alpha(\omega) \equiv \left.\frac{d\ln\left\langle \Delta r^2(t)\right\rangle}{d\ln t}\right|_{t=1/\omega}$

Standard errors were estimated using bootstrap analysis (6).

Brownian dynamics simulation-List of parameter values used to generate Figs. 4, 5, S5 and S6:

Spring equilibrium length r_{eq} =100 nm

Distance between beads in an adhesion r_{FA} = 60 nm (Fig. 4); r_{FA} =55 nm (Fig. 5, S5 and S6)

Distance between adhesion nuclei d = 500 nm (Fig. 4); d = 200 nm (Fig. 5, S5 and S6)

Spring constant $K = 1000\ k_BT/r_{eq}^2 = 4.27\times10^{-4}\ N/m$ ($K = 200\ k_BT/r_{eq}^2$ for Fig. 5A)

Viscosity $\eta = 200 Pa\times\sec$

Friction ξ= 290 $k_BT\times\sec/r_{eq}^2 = 1.25\times10^{-4}\ N\times\sec/m$

Cell diameter = 10 μm

Force pulse frequency w_F = 1 Hz

Force pulse duration = 3 sec

Force pulse amplitude = 20 pN

Simulation time step Δt = 10 milliseconds

aECM

M-MASMTGGQQMG-HHHHHHH-DDDDK(LD-YAVTG**Fn10m**SPASSKIA((VPGIG)$_2$VPG*K*G(VPGIG)$_2$)$_4$VP)$_3$-LE

T7 tag | His tag | Cleavage site | cell-binding domain | Elastin-like domain

FN10m:

VSDVPRDLEVVAATPTSLLISWDAPAVTVRYYRITYGETGGNSPVQEFTVPGSASTATISGLAPGVDYTIT
VYAVTG**RGD**SPASSAPISINYR

Fig. S1 Amino acid sequence of aECM protein containing the tenth fibronectin Type III domain. The aECM protein contains a T7 tag, a hexahistidine tag, an enterokinase cleavage site, and elastin-like domains containing lysine residues (italicized) for crosslinking.

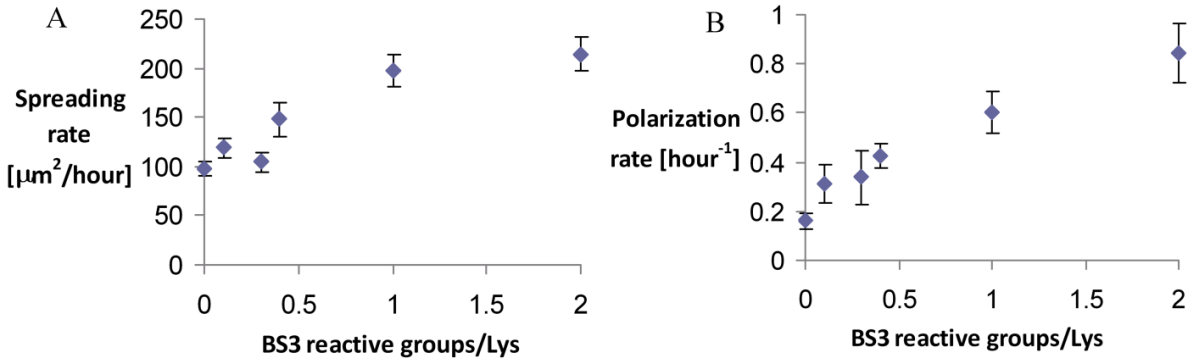

Fig. S2: The rates of CHO-K1 cell spreading (A) and polarization (B) as functions of crosslink density (i.e., the ratio of equivalents of BS3 reactive groups to equivalents of lysine residues). Error bars represent s.e.m.

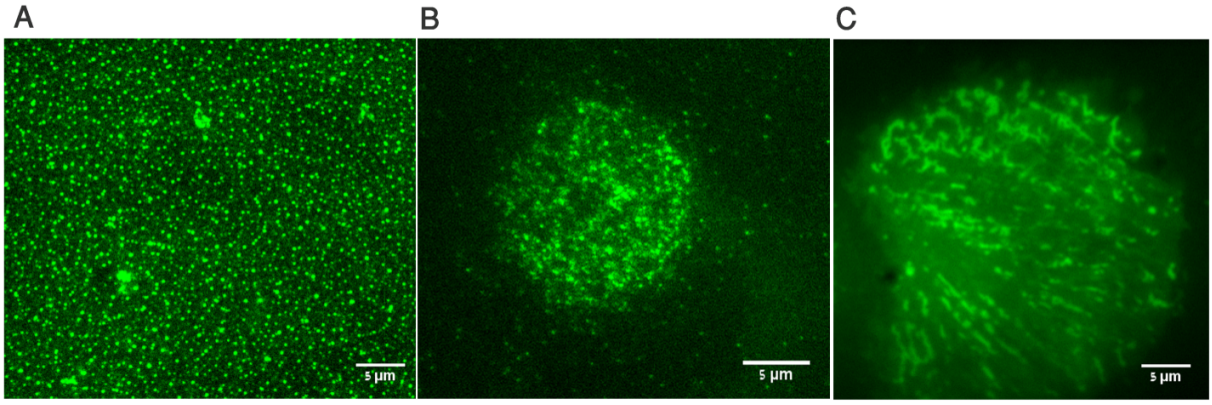

Fig. S3 *p*-Azidophenylalanine residues in an aECM protein similar to that shown in Fig. S1 (7, 8) were labeled with BODIPY 488-cyclooctyne (a gift from Dr. John D. Fisk, (9)). Representative TIRFM images of the distribution of aECM-bound dye molecules before (A) and after (B and C) plating of CHO-K1 cells. The cells (which are not fluorescent) are in an initial stage of spreading in (B) and well spread in (C). The protein was crosslinked by 2 min UV irradiation (see (7, 8)). In (B) and (C) the dye is most visible in the regions occupied by cells. Dye in the surrounding areas is not as bright, but is readily detected at higher gain.

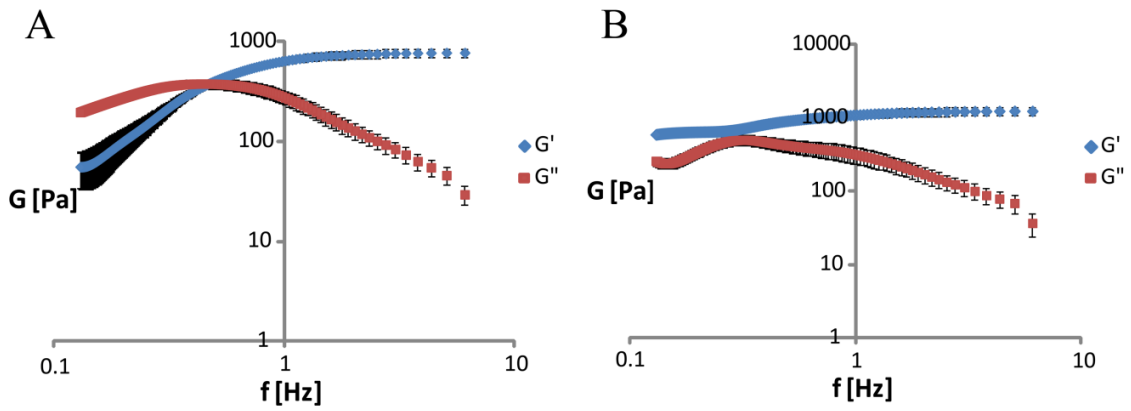

Fig. S4: Frequency-dependent storage (G') and loss (G") moduli for aECM1:0 (A) and aECM1:2 (B) obtained from microrheology measurements (3, 4, 10). Error bars were estimated using bootstrap analysis (6). The relevant frequency window is that in which cells act to deform the matrix, which is not known for CHO cells. For the purposes of comparing matrices, we focused on the range of frequencies (0.1-10 Hz) characteristic of the beating of cardiac cells (11, 12) and membrane ruffling (13).

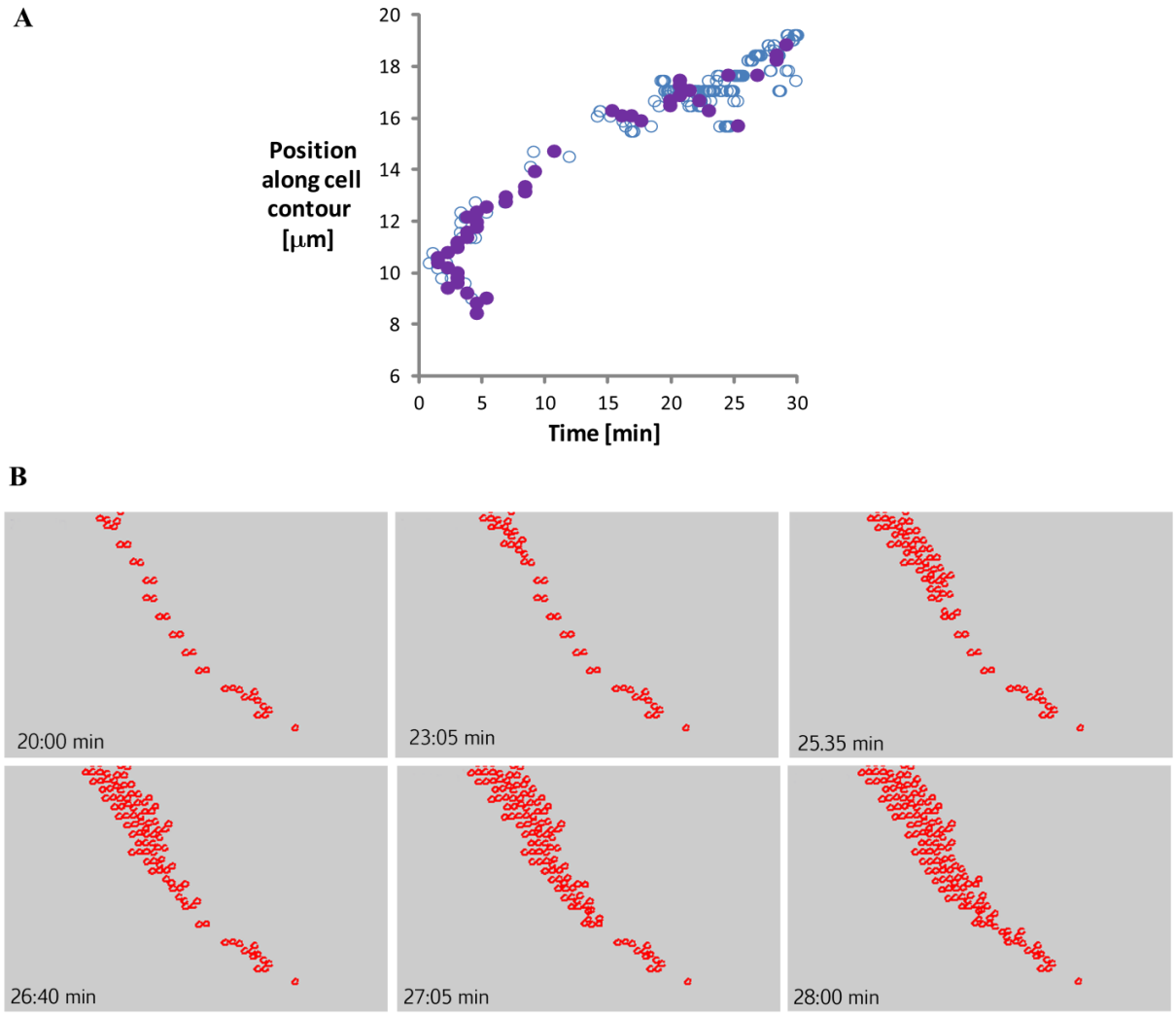

Fig. S5 Dynamics of cell adhesion growth obtained by Brownian dynamics simulation with $r_{FA} = 0.55 r_{eq}$ and $d = 200nm$. (A) Position of maximal growth rate (filled circles) and maximal compressive deformation (empty circles) along the cell contour as a function of time. (B) The corresponding snapshots from the simulation. Only a small part of the cell contour is shown, and only the beads that are part of an adhesion complex are displayed. Notice that adhesions grow sequentially along the cell contour (see also Video S4).

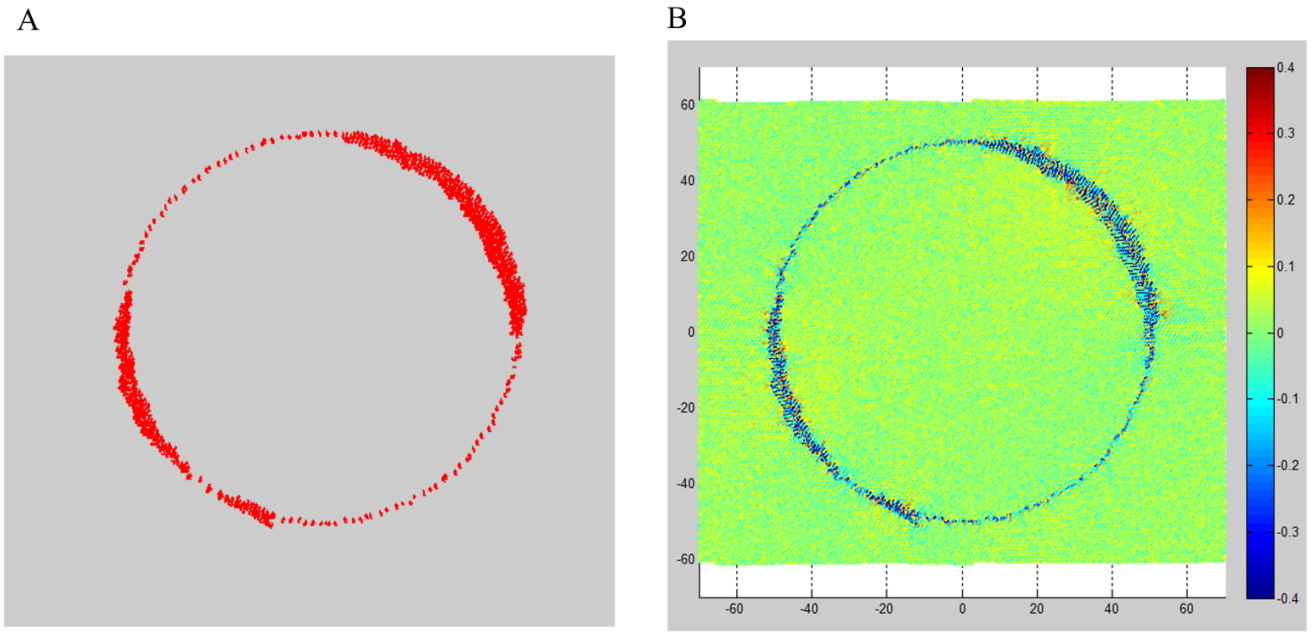

Fig. S6 Adhesion configuration (A) and material deformation (B) for the case of a small simulation box (140 x 140 beads, $r_{FA} = 0.55 r_{eq}$, $d = 200nm$). In A only the beads that are part of an adhesion are shown. All numbers are in units of r_{eq}. The deformations are defined for each spring as: $\left(r - r_{eq}\right)/r_{eq}$ where r is the length of the spring. Positive values correspond to extension; negative values correspond to compression. The polarized configuration of cell adhesions is a result of coupling between the opposite edges of the cell, mediated by material deformation. Deformation caused by adhesion formation at the "top" edge of the cell deforms the material at the "bottom" edge of the cell as a consequence of the periodic boundary condition. The size of the simulation box corresponds to the effective cell density. The configuration shown here corresponds to high cell density, which allows cells to communicate by deforming the material and synchronizing their polarization states.

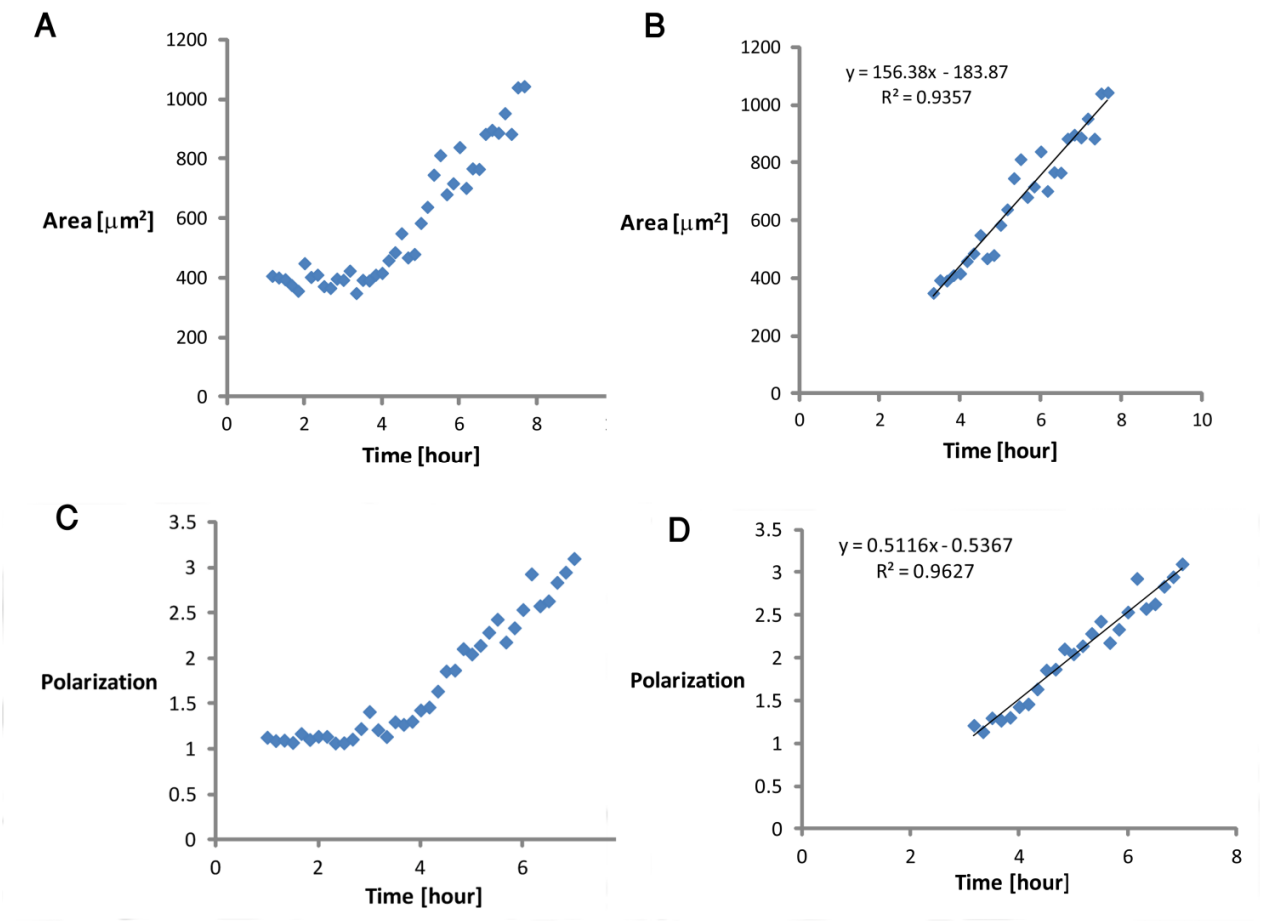

Fig. S7 Representative plots of cell projected area (A) and polarization (C) as a function of time for aECM1:2. (B) and (D) are the corresponding linear fit to the spreading and polarization phases of the curve respectively.

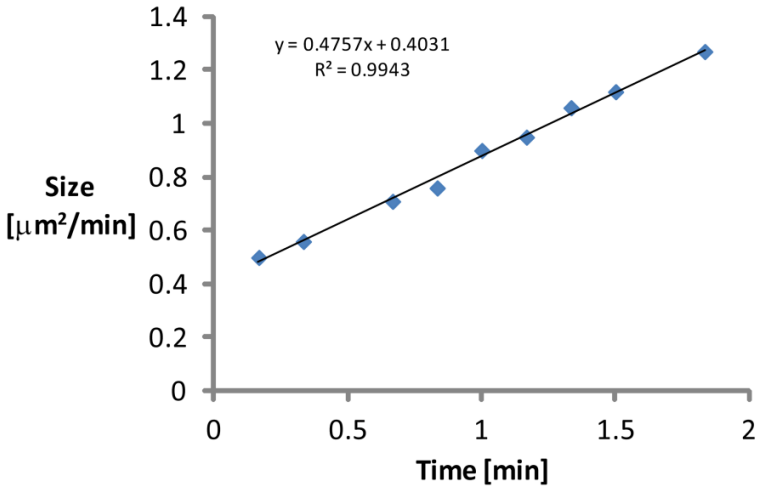

Fig. S8 A representative plot of adhesion size as a function of time for aECM1:2.

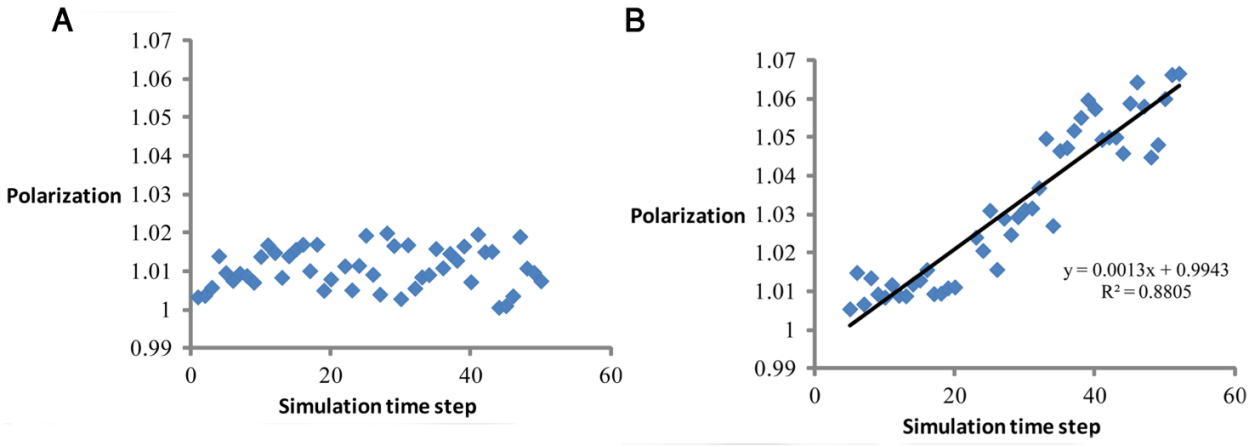

Fig. S9 Cell polarization for soft (A; $K = 200\ k_B T / r_{eq}^2$) and rigid (B; $K = 1000\ k_B T / r_{eq}^2$) matrices as obtained by Brownian dynamics simulations. These plots correspond to videos S5 and S6. Cell polarization (cell aspect ratio) was calculated by finding the minimum area ellipse

that includes all adhesion complexes, and determining the ratio of major and minor axes of the ellipse.

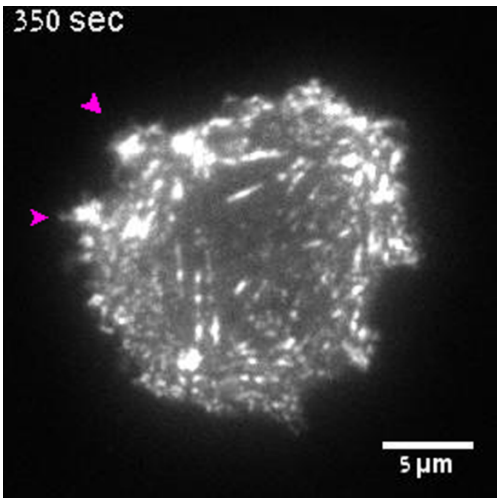

Videos S1 Dynamics of paxillin/eGFP-labeled adhesions during spreading of CHO-K1 cells on highly crosslinked aECM substrate (aECM1:2). Images of paxillin/eGFP were collected every 10 sec using TIRF microscopy. The pink arrows indicate the position of maximal adhesion growth rate. Notice that the maximal adhesion growth rate travels along the cell contour. Video S1 corresponds to Fig. 2.

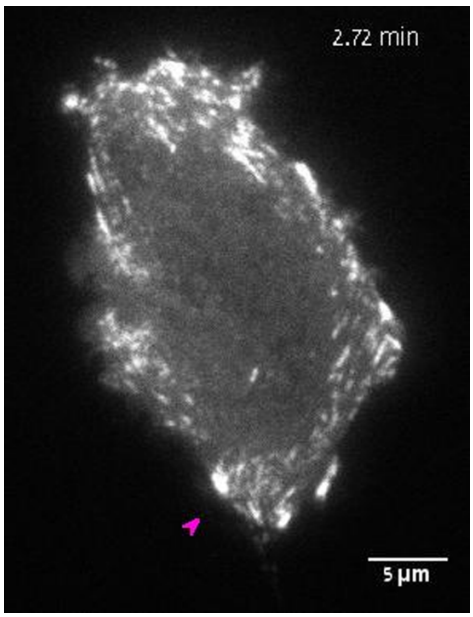

Videos S2 Dynamics of paxillin/eGFP-labeled adhesions during spreading of CHO-K1 cells on highly crosslinked aECM substrate (aECM1:2). Images of paxillin/eGFP were collected every 10 sec using TIRF microscopy. The pink arrows indicate the position of maximal adhesion growth rate. Notice that the maximal adhesion growth rate travels along the cell contour.

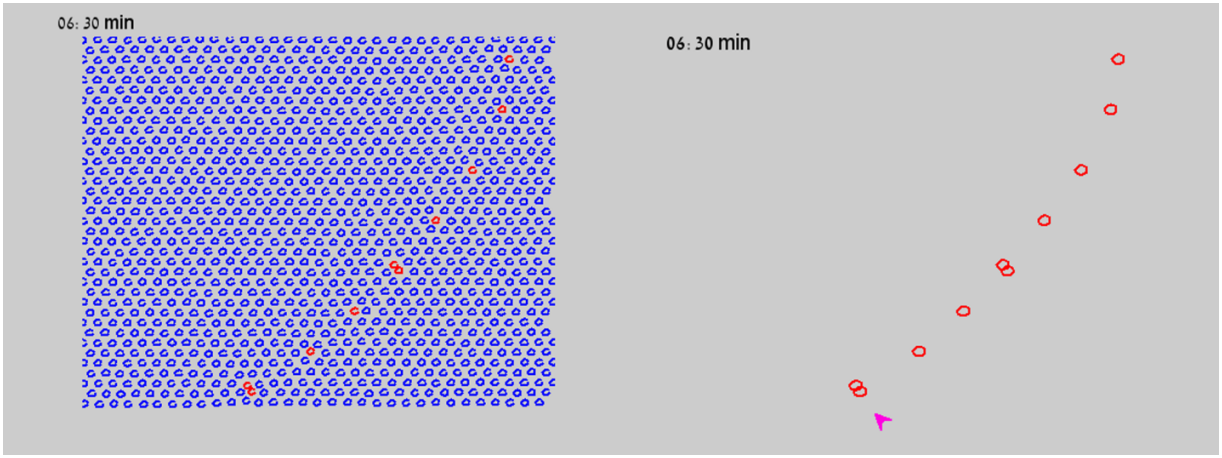

Video S3 Dynamics of adhesion growth obtained by Brownian dynamics simulation with $r_{FA} = 0.6 r_{eq}$ and $d = 500nm$. A small part of the cell contour is shown. The Video corresponds to Fig. 4. *Left:* Beads that are part of an adhesion complex are shown in red. Beads that are not part of an adhesion complex are shown in blue. Adhesion growth is represented by aggregation of beads; a bead that joins an adhesion complex turns from blue to red. *Right:* Only beads that are part of an adhesion complex are shown. The pink arrows indicate the position of maximal adhesion growth rate. Notice that adhesions grow sequentially along the cell contour.

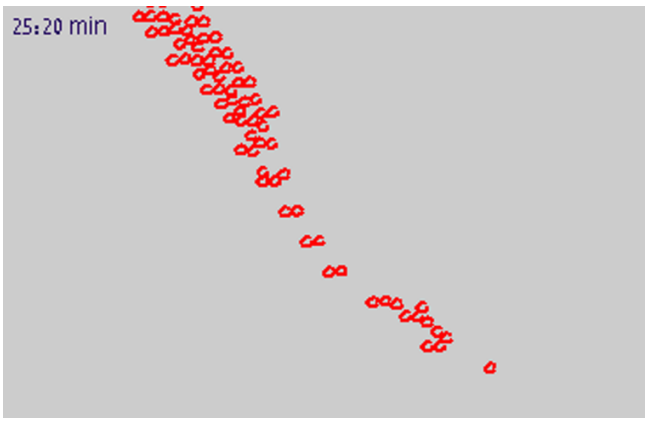

Video S4 Dynamics of cell adhesion growth obtained by Brownian dynamics simulation with $r_{FA} = 0.55 r_{eq}$ and $d = 200nm$. A small part of the cell contour is shown. The video corresponds to Fig. S5. Only beads that are part of an adhesion complex are shown. Notice that adhesions grow sequentially along the cell contour.

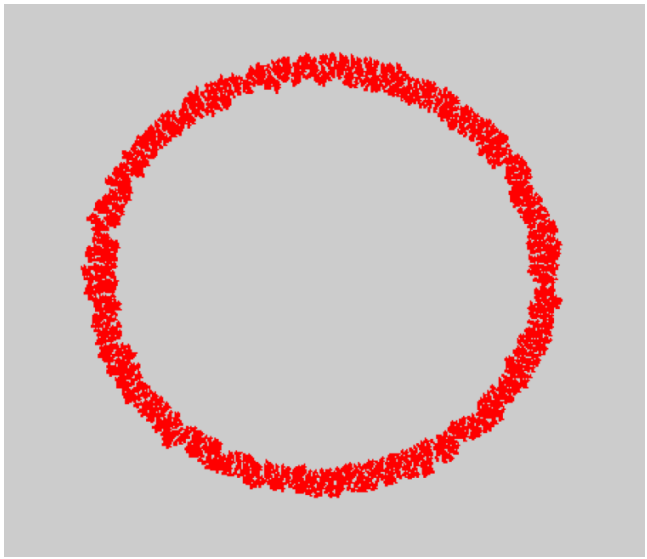

Video S5 Dynamics of cell adhesion growth for soft matrix obtained by Brownian dynamics simulation with $r_{FA} = 0.55 r_{eq}$ and $d = 200nm$. The video corresponds to Fig. 5A and Fig S9-A. Only beads that are part of an adhesion complex are shown.

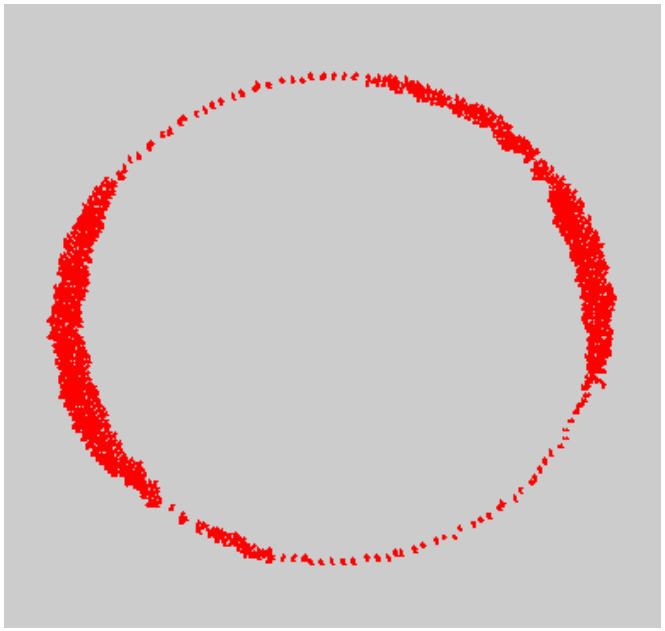

Video S6 Dynamics of cell adhesion growth for rigid matrix obtained by Brownian dynamics simulation with $r_{FA} = 0.55 r_{eq}$ and $d = 200nm$. Only beads that are part of an adhesion complex are shown.

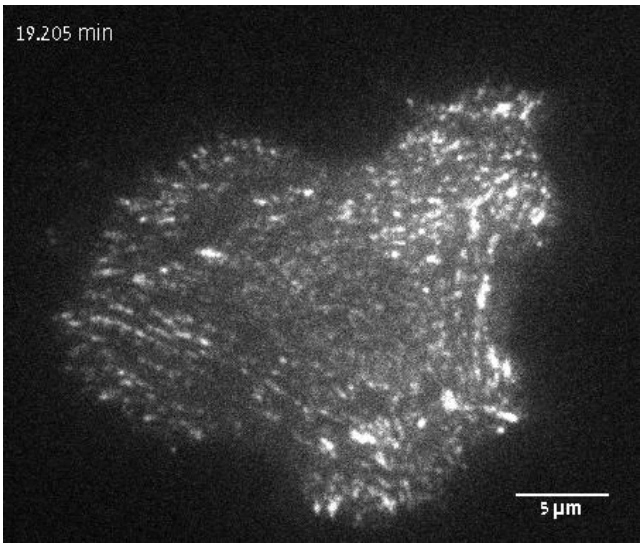

Videos S7 Dynamics of paxillin/eGFP-labeled adhesions during spreading of CHO-K1 cells on uncrosslinked aECM substrate (aECM1:0). Images of paxillin/eGFP were collected every 10 sec using TIRF microscopy.

References

1. Thompson RE, Larson DR, & Webb WW (2002) Precise nanometer localization analysis for individual fluorescent probes. *Biophys J* 82:2775-2783.
2. Kural C, Balci H, & Selvin PR (2005) Molecular motors one at a time: FIONA to the rescue. *J Phys Condens Matter* 17:S3979-S3995.
3. Wirtz D (2009) Particle-Tracking Microrheology of Living Cells: Principles and Applications. *Annu Rev Biophys* 38:301-326.
4. Mason TG & Weitz DA (1995) optical measurements of frequency-dependent linear viscoelastic moduli of complex fluids. *Phys Rev Lett* 74:1250-1253.
5. Mason TG (2000) Estimating the viscoelastic moduli of complex fluids using the generalized Stokes-Einstein equation. *Rheol. Acta* 39:371-378.
6. Efron B & Tibshirani RJ (1993) *An introduction to the bootstrap* (Chapman & Hall/CRC, Boca Raton).
7. Nowatzki PJ, Franck C, Maskarinec SA, Ravichandran G, & Tirrell DA (2008) Mechanically tunable thin films of photosensitive artificial proteins: Preparation and characterization by nanoindentation. *Macromolecules* 41:1839-1845.
8. Carrico IS, *et al.* (2007) Lithographic patterning of photoreactive cell-adhesive proteins. *J Am Chem Soc* 129:4874-4875.
9. Beatty KE, Szychowski J, Fisk JD, & Tirrell DA (2011) A BODIPY-Cyclooctyne for protein imaging in live cells. *Chembiochem* 12:2137-2139.
10. Mason TG, Ganesan K, vanZanten JH, Wirtz D, & Kuo SC (1997) Particle tracking microrheology of complex fluids. *Phys Rev Lett* 79:3282-3285.
11. Engler AJ, *et al.* (2008) Embryonic cardiomyocytes beat best on a matrix with heart-like elasticity: scar-like rigidity inhibits beating. *J Cell Sci* 121:3794-3802.
12. Werdich AA, *et al.* (2008) Differential effects of phospholamban and Ca2+/calmodulin-dependent kinase II on [Ca2+]i transients in cardiac myocytes at physiological stimulation frequencies. *Am J Physiol Heart Circ Physiol* 294:H2352-H2362.
13. Giannone G, *et al.* (2004) Periodic lamellipodial contractions correlate with rearward actin waves. *Cell* 116:431-443.